# Effect of Damage and Support Damping Mechanisms on Unimorph Piezoelectric Energy Harvester

Khazaee, Majid; Rezaniakolaei, Alireza; Rosendahl, Lasse

*Published in:*
Journal of Vibration and Control

*DOI (link to publication from Publisher):*
10.1177/1077546319855162



*Publication date:*
2019

*Document Version*
Accepted author manuscript, peer reviewed version

# Effect of Damage and Support Damping Mechanisms on Unimorph Piezoelectric Energy Harvester

Majid Khazaee, Alireza Rezania*, Lasse Rosendahl

Department of Energy Technology, Aalborg University, Pontoppidanstræde 111, 9220 Aalborg East, Denmark



**Abstract**

Damping plays a critical role in power generation by piezoelectric energy harvesting (PEH), and yet there is the lack of sensitivity studies on different sources of damping. In this paper, two damping sources in unimorph PEH, namely support loss and damage damping mechanisms are experimentally investigated. Variation of the power generation are evaluated with respect to the sources of damping. Accordingly, the power generation model is developed according to the experimental results in this work and using a single degree of freedom analytical model. This study has focus on debonding effect, as an internal damping source, and support loss, as a critical source of external energy dissipation. The results show that the debonding reduces the output power dramatically at resonance and, particularly, at anti-resonance frequencies. Moreover, investigation of the support loss shows that material of clamp as well as installation torque have an impact on the support loss and, consequently, affect the output power.

**Keywords:** Piezoelectric Energy Harvesting, Unimorph, Damping Effect, Debonding Effect, Support Loss.

## 1. Introduction

With the recent development in electronics, e.g. the decrease in power consumption (Khaligh et al., 2010), low power energy harvesting from thermal and kinetic sources of energy is being widely

* Corresponding author: Alireza Rezaniakolaei. E-mail: alr@et.aau.dk

considered as an essential tool to introduce self-powered devices for elaborating system abilities in terms of life time and accessibility of remote systems (Ahmed et al., 2017). Furthermore, energy harvesting systems can be manufactured using additive manufacturing techniques (Mortazavinatanzi et al., 2018) for non-flat surfaces with flexible ink-based (Https://www.piezotech.eu, n.d.; Qing et al., 2018). Among the energy harvesting mechanisms, piezoelectric energy harvesters (PEHs) have drawn much attention due to structure simplicity and ease of integration into the host structure (Khazaee et al., 2019). Piezoelectric materials can be grouped into three types, ceramic, polymer, and composite types (Ahmed et al., 2017). Macro-Fiber Composite (MFC) with ceramic fibers is a composite material with excellent electromechanical properties of ceramics as well as polymeric flexibility (Khazaee et al., 2019), that makes it ideal material for long-endurance kinetic energy harvesting.

Unimorph geometry is one of the most widely used configuration for PEHs (Li et al., 2014), in which one piezoelectric layer is bonded into a non-piezoelectric substrate shim with clamped-free boundary condition. A number of researchers used MFC materials for PEH in unimorph configuration (Erturk et al., 2008; Khazaee et al., 2019; Shan et al., 2015; Sodano et al., 2006). Shan et *al.* (Shan et al., 2015) used a bonded beam from MFC and polyvinyl chloride layers in clamp-free boundary condition. The beam was subjected to water vertexes induced from an upstream cylinder for PEH and obtained a maximum output power of 1.32 μW. Moreover, by an experimental study, Sodano et *al.* (Sodano et al., 2006) compared the maximum instantaneous power of three types of materials in unimorph geometry, including the MFC material, over 12 bending modes and obtained 11.714 μW at third bending mode. Obtaining maximum power from vibration sources is the main research subject within PEHs. Reddy et al. (Reddy et al., 2016) introduced a cavity inside the substrate beam in order to enhance harvested power from PEHs. In the context of power estimation, it is a well-known fact that damping has a critical role on the output power by PEHs (Roundy et al., 2003). Four factors contribute into energy dissipation of unimorph PEHs, namely energy dissipation from air resistance force, squeeze force, internal energy dissipation and support loss (Hosaka et al., 1995).

Internal energy dissipation in composite structures is a parameter influenced by five factors, namely matrix or fiber viscoelasticity, interphase, damage, viscoplastic, and thermoelastic (Bhattacharjee and Nanda, 2018; Chandra et al., 1999). In almost all numerical and experimental studies on PEHs, a perfect bonding have been assumed, while adhesion loss or debonding due to the aging or improper manufacturing process is a major concern about adhesive joints (Pazand and Nobari, 2017). Saravanos and Hopkins (Saravanos and Hopkins, 1996) showed that delamination cracks between layers of a composite beam increases modal damping of the beam. Although debonding can have a substantial effect on damping (Khazaee et al., 2018) and consequently will change the PEH power dramatically, yet there is no investigation on effect of this damage on the output power.

Support loss, also called clamping loss, is the energy dissipated from a vibrating structure through its support. As the structure undergoes flexural vibration, it excites its support both by shear and moment forces causing elastic wave propagating into the support, which consequently leads to energy absorption by the support (Hao et al., 2003). Chen et *al.* (Chen et al., 2017) looked at the support loss in micro-electromechanical systems and introduced it as the inverse of quality factor, which can be obtained through elastic wave propagation through the support. Although all the cantilever clamps are created by screw joints, these studies (Chen et al., 2017; Hao et al., 2003) did not consider the effect of joint characteristics on the support loss. If the joints are used to provide clamps, then friction regions due to the bolted joints may cause slipping, which is a source of damping (Goyder, 2018). An important source of energy dissipation in bolted joints is joint tightness. High clamping pressure produces greater penetration forces (Ibrahim and Pettit, 2005). Since unimorph geometry is built by clamping piezoelectric harvester with the screw, any source of energy dissipation in the clamps, including joint tightness, should be considered for investigation of power generation by a piezoelectric.

Within energy harvesting research area, which is highly dependent on the different aspects of vibrational characteristics of the device, there is lack of studies investigating the dependency of the power to vibrational features within the system such as damage and support damping mechanisms. Thus, in this paper a series of experimental studies are carried out to investigate the effect of debonding, as one of the regular defect in adhesive layers, and support loss on output power of a composite beam with MFC piezoelectric layer. In addition, using a single degree of freedom method, change of the power with respect to debonding and support loss is modelled as the damping variation within the system.

## 2. A Modeling Technique for Unimorph Harvester

There are various techniques for modelling piezoelectric energy harvesters ranging from simple one degree of freedom (1-D) to two-dimension multi degree of freedom methods. While 1-D methods require less parameters to model the system, other methods require more parameters to be defined and are computationally time consuming. On the other hand, as proposed by Erturk and Inman (Erturk and Inman, 2008), a 1-D method that considers electro-mechanical coupling can be a suitable method for assessment the behavior of a piezoelectric harvester. Moreover, 1-D methods were previously used for studying piezoelectric energy harvesters by researchers (DuToit et al., 2005; DuToit and Wardle, 2007; Roundy et al., 2003). As in this paper experimental data and analytical model will be correlated for obtaining damping coefficient in many case studies, it is desirable to keep the model as simple as possible and at the same time accurate. Hence, a 1-D model with electro-mechanical coupling will be handled into a suitable form for our investigation by elaborating damping coefficient in this model. In the result section, the accuracy of the model to predict experimental data will be presented. Figure 1 presents the schematic of the model, which comprises a piezoelectric mass with internal resistance of $R_p$, and a proof mass simply connected to a load resistor, $R_l$. This model is valid for the case that there is no substrate shim. In order to comprise effect of the substrate, a coefficient, $\alpha_m$, which is the proportion of piezoelectric mass to device mass, is added. Therefore, the equations of motion for a piezoelectric harvester with the substrate and piezoelectric layer can be shown as (DuToit et al., 2005):

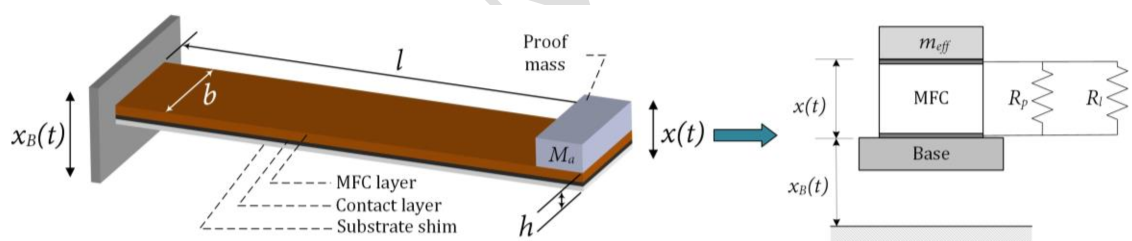


*Figure 1. Single degree of freedom electromechanical model* (DuToit et al., 2005)

$$\ddot{x}(t) + 2\,\zeta_m \omega_n \dot{x}(t) + \omega_n^2\, x(t) - \alpha_m \omega_n^2 d_{31} V_p(t) = -\ddot{x}_B(t) \tag{1}$$

$$R_{eq} C_p \dot{V}_p(t) + V_p(t) + m_{eff} R_{eq} d_{31} \omega_n^2 \dot{x}(t) = 0 \tag{2}$$

, where $\ddot{x}_B$ [m/s$^2$] is the base excitation acceleration, $x$ [m] is the relative displacement of harvester tip respect to the base, $\omega_n$ [1/rad] is the undamped natural frequency of harvester defined as $\sqrt{k/m_b}$, $\zeta_m$ is the mechanical viscous damping ratio, $V_p$ [V] is the output voltage and $m_{eff} = M_a + m_p/3$ [kg] (DuToit et al., 2005) is the effective mass of piezoelectric layer contributed to shunt damping effect. The overhead dot indicates the time derivative. In addition, $d_{31}$ [C/N] is the piezoelectric coupling coefficient in 3-1 mode, $R_{eq}$ [Ω] is the equivalent electric resistance, $C_p$ is the capacitance of the piezoelectric. The capacitance is defined in terms of dielectric constant $K$, the permittivity of free space ($\varepsilon_0$=8.9 nF/m), piezoelectric area $A_p$ [$\mathrm{m}^2$] and thickness $t_p$ [m] with $C_p=K\,\varepsilon_0\,A_p/t_p$.

If the base excitation is assumed to be harmonic, $\ddot{x}_B(t) = \bar{X}_B e^{j\omega t}$, then the displacement and voltage will be a harmonic function with the same frequency but with different phase, e.g. $V_p(t) = \bar{V}_p e^{j\omega t+\varphi}$ and $x(t) = \bar{X} e^{j\omega t+\varphi}$. By defining magnitude of power to be $\bar{P}_{out} = \left(\bar{V}_p\right)^2/R_{eq}$, it can be expressed as (DuToit et al., 2005):

$$\left|\frac{\bar{P}_{out}}{\bar{X}_B}\right| = \frac{(1/\omega_n)\, m_{eff}\, r\, k_e^2 \left(R_{eq}/R_l\right)_{31} \Omega^2}{\sqrt{\left[\left(1-(1+2r\zeta_m)\Omega^2\right)^2 + \left((2\zeta_m\Omega)+\left(r\Omega - r\Omega^3\right)+\alpha_m r k_e^2 \Omega\right)^2\right]}}, \tag{3}$$

where $r = R_{eq}\omega_n C_p$ is dimensionless resistance term, $\Omega = \omega/\omega_n$ is dimensionless frequency, and $k_e$ is the electromechanical coupling factor defined with $k_e^2 = k_{31}^2/(1-k_{31}^2)$. As it can be seen from Eq.(3), apart from physical properties of piezoelectric harvester, output voltage depends on load resistance and excitation frequency for a given excitation magnitude. Output power from piezoelectric is maximum at an optimum load resistance called optimum load, $R_{opt}$. Moreover, if the maximum power at short-circuit and open-circuit conditions is plotted against frequency, two frequencies are assigned to maximum power that are called short-circuit, $\omega_{sc}$, and open-circuit resonant frequencies, $\omega_{oc}$, respectively. According to these values, one can calculate the electromechanical coupling factor, $k_e$, of piezoelectric harvester with $k_e^2 = \sqrt{(\omega_{oc}/\omega_{sc})^2 - 1}$.

The presented model is a simple 1-D model. However, because output power obtained by this method is expressed in terms of coefficients that will be obtained experimentally, see Eq.(3), the model will present accurate data compared to the experimental data, as was proved in (DuToit and Wardle, 2007). For example, $\omega_n$ can be obtained through experimental tests and by evaluating $\omega_{oc}$ and $\omega_{sc}$ through measurements of power over a wide frequency range, $k_e$ will be accordingly calculated. The only parameter that should be investigated is damping coefficient. The analytical model assigned a single coefficient, e.g. $\zeta_m$, for considering energy dissipation in the energy harvesting system in cantilever configuration. On the other hand, in the presented study, it is aimed to capture the effects of two sources of damping mechanisms, e.g. damage damping and support loss, which have different natures. Thus, to make the damping model closer to the actual one, all sources of energy dissipation in the system will be identified and then all the other damping mechanisms apart are evaluated analytically while damage and support loss damping will be extracted according to the measurements.

Energy dissipation consists of internal energy dissipation, fluid-structural viscous damping and support loss due to the cantilever boundary condition and for the case of deboned sample, a damaged damping term should be considered. These sources of energy dissipation are shown in Figure 2. So, $\zeta_m$ can be expressed with Eq. (4).

$$\zeta_m = \zeta_{Structural} + \zeta_{Fluid-Structure} + \zeta_{Support} + \zeta_{Damage} \tag{4}$$

Fluid-structural damping, $\zeta_{Fluid-Structure}$ , is considered to be due to airflow force due to vibration of beam in free air and squeeze force due to airstream force from the near fixed boundary wall. Internal energy dissipation, $\zeta_{Structural}$ , is the energy dissipated inside material, which is an energy dissipation source inside the beam. Fluid-structural damping terms are more straightforward to deal with and some analytical formula were reported for them, such as (Hosaka et al., 1995), as it is less difficult to estimate the resistance force against beam transverse vibration induced from surrounded fluid. On the other hand, damage ( $\zeta_{Damage}$ ) and support loss ( $\zeta_{Support}$ ) mechanisms are difficult to deal with and are often measured according to experimental data. In this research, fluid-structural and internal energy dissipation mechanisms are calculated according to analytical expressions see Eq. (5) (Hosaka et al., 1995), and the support loss and damage damping mechanisms are evaluated based on experimental data.

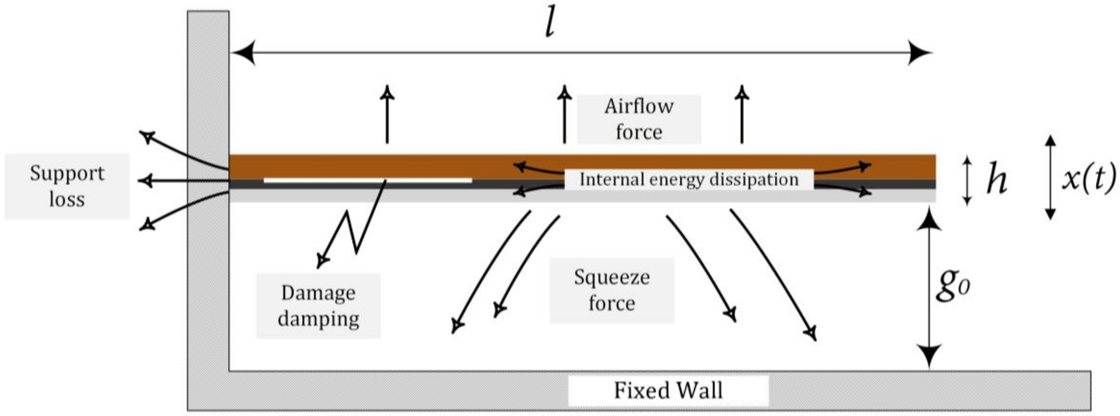


*Figure 2. Different sources of energy dissipation considered in this study*

$$\zeta_{Fluid-Structure} = \frac{\mu b^2}{2\rho_b g_0^3 h \omega_n} + \frac{\frac{3}{4}\pi b^2 \sqrt{2\rho_{air}\mu\omega_n}}{2\rho_b hbl\,\omega_n} \qquad (5)$$

$$\zeta_{Structural} = \eta/2$$

where $\mu$ and $\rho_{air}$ are dynamic viscosity and density of air. In addition, $g_0$ is the distance between the fixed wall and beam outer surface as shown in Figure 2 and $\eta$ is the structural damping coefficient and in this study a value of $0.5\times10^{-6}$ is considered (Blom et al., 1992).

Due to the presence of damping in the equation for output power, Eq. (3), damping will have a significant effect on the output power in a unimorph energy harvester. This work aims to investigate the effect of changing the damping coefficient, $\zeta_m$, through debonding and the support tightness, on the output power while four damping mechanisms are considered in the presented study, see Eq. (4). Hence, it is necessary to capture the actual variation of the energy dissipation source under study. In section 4, support loss damping will be evaluated from the defect-free state, which this value will be used for the deboned state and hence the actual damage damping due to debonding will be evaluated. In section 5, there is no damage damping and support damping can be directly evaluated from experimental data.

## 3. Experimental Procedure

The effects of the debonding and support loss on the output power were investigated through experiments. The experiments were carried out with piezoelectric samples in unimorph geometry. The piezoelectric samples were clamped with a clamp box on one end. Then, it is excited with a magnetic vibration shaker by sinusoidal input signal, where its response in terms of output voltage and current were recorded. Figure 3 shows the configuration of the piezoelectric energy harvesters throughout the study.

The piezoelectric layer is a MFC with elastic modulus of 30.336 GPa and 15.857 GPa in x- and y-directions, respectively, and Poisson's ratios of 0.31 in xy and 0.16 in yx and shear modulus of 5.515 GPa. Thickness of the MFC is 0.30 mm while the thickness of the PZT fibers are 190 µm with density of active area of 5.44 g/cm$^3$. The electromechanical properties of the piezoelectric layer are $d_{33}$= 460 pC/N, and $d_{31}$= -210 pC/N. The center shim is made of aluminum with thickness of 0.12 mm, elastic modulus of 68.9 GPa and density of 2.7 g/cm$^3$. The piezoelectric layer is bonded to the center shim with epoxy rapid 332 adhesive with density of 1.16 g/cm$^3$. In the case of investigating debonding effects in section 4, thickness of bond layer in perfect and poorly cured bond conditions are 400 and 189 µm, respectively. In section 5, where the effect of support loss damping is investigated, the bond layer thickness equals to 245 µm.

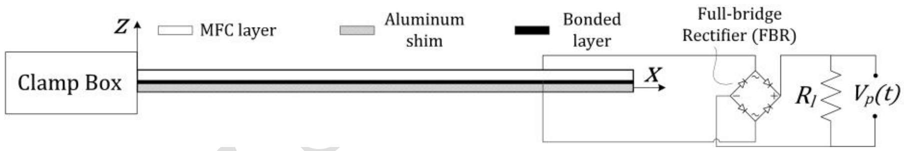


*Figure 3. Piezoelectric energy harvester configuration*

The aforementioned unimorph energy harvester is excited with a VSD 201 Shaker while its input voltage and electrical power are measured. Signal generation and data recording were carried out with National Instrument modules. For signal generation, NI 9263 module, a 4-channel ±10 V 16-Bit Analog Voltage Output, which is adjusted by LabVIEW™ 2013 is connected to a Kepco AC power generation and the output from Kepco power supply is wired to the shaker. A NI 9215 module with 4-channel ±10 V 16-Bit Analog Voltage Input is used for recording voltage output of the piezoelectric harvester. A National Instrument Compact data acquisition system (cDAQ) type 9172 is used as the medium between the modules and experimental components, e.g. the shaker and piezoelectric samples. Figure 4 shows the experimental setup.

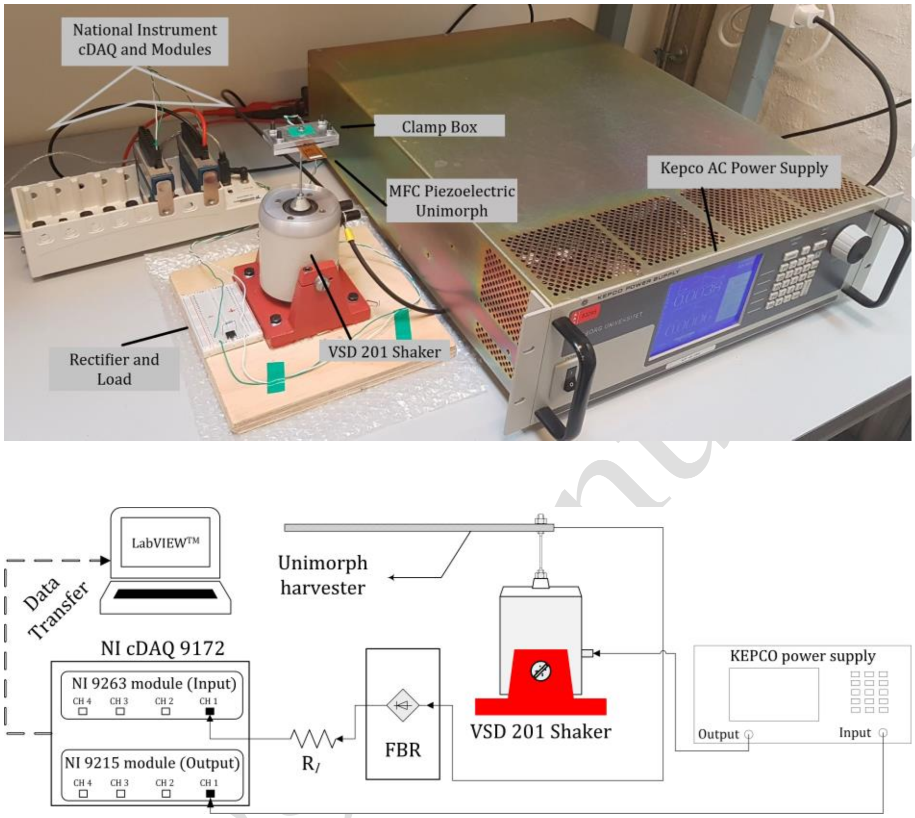


*Figure 4. Setup for measuring voltage output*

## 4. Debonding Effects

During the model derivation for the piezoelectric energy harvester from vibration, mostly cantilever configuration is considered with the perfect bonding between piezoelectric and metal substrate. In practice, the perfect bonding assumption may be degraded over time during operation or during manufacturing process in the first stage (Pazand and Nobari, 2017). In particular, as the loading condition is dynamic and the harvester mostly vibrates close to its fundamental natural frequency, it is likely to observe debonding between the substrate and the piezoelectric layer. The debonding might have two influences on the output power. An obvious effect is that, it prevents the vibration of a part of the energy harvester, so it will reduce the active area for power generation. Moreover, the debonding may increase the damping ratio of the device, which results to less power generation. This increment in the damping depend on the vibration mode (Khazaee et al., 2018). In this section, an experimental verification of the debonding effect on the output power is presented.

Two samples are tested with the same length and width, each consisting of a 0.3 mm thickness MFC piezoelectric layer. The samples are bonded to an aluminum substrate with 0.12 mm thickness by epoxy rapid 332 adhesive. The thickness of bond layers are 400 and 189 µm in pristine and poorly cured bond samples, respectively. Figure 5 shows the pristine and debonded samples with capacitance of $C_p$=177.07 nF/m for an active length of 85 mm. The piezoelectric harvester is connected to a 31500-Ω resistance load. The unimorph is excited over frequency range of 5 to 100 Hz with 1 Hz frequency step with the same excitation amplitude. Three replications are used to show the repeatability of tests.

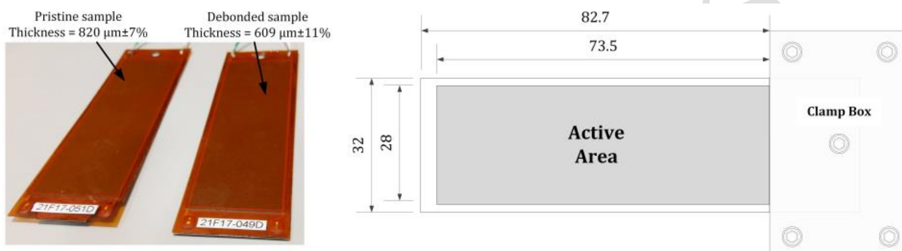


*Figure 5. MFC pristine and debonded dimensions and unimorph configuration with clamp box screws*

As can be interpreted from Figure 5, thickness of the adhesive layer for one sample was considered 211 µm less than the other sample to make it vulnerable to debonding due to inappropriate debonding thickness. Then, the sample was excited by the shaker on its natural frequency until a debonding area is initiated and developed. It is worth mentioning that after initiation of the debonding, the propagation was quick. The samples were scanned using Acoustic Microscope KSI V8 from the aluminum substrate and from MFC layer down to the other front side to find out the layers within them debonding is occurred. Figure 6 shows the Acoustic Microscope KSI V8 for scanning the samples from the aluminum side.

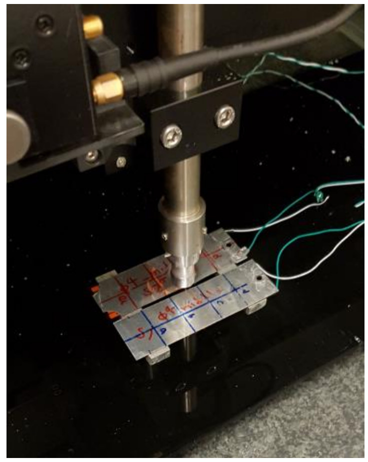

*Figure 6. Pristine and debonded samples scanned with Acoustic Microscope KSI V8*

Figure 7 shows the scanned pictures of the samples in depth with ultrasonic waves. Areas with different colors in Figure 7 represent the regions with different densities. In order to recognize debonding regions, similar regions with different colors should be observed at different depth levels. It has been observed that, the debonding was initiated between aluminum shim and adhesive layer, as the color scattering in the surface can be seen from Figure 7 (b) through (c). Since the dark color regions exist at different depths, from Figure 7 (a)-(e), this area is the likelihood-debonding region. This region is marked with white box in Figure 6. In addition, there are two regions with distinctive colors on the Figure 7 (e)-(f) on the pristine sample, which based on thickness measurements is found to be the result of higher density of adhesive in these regions.

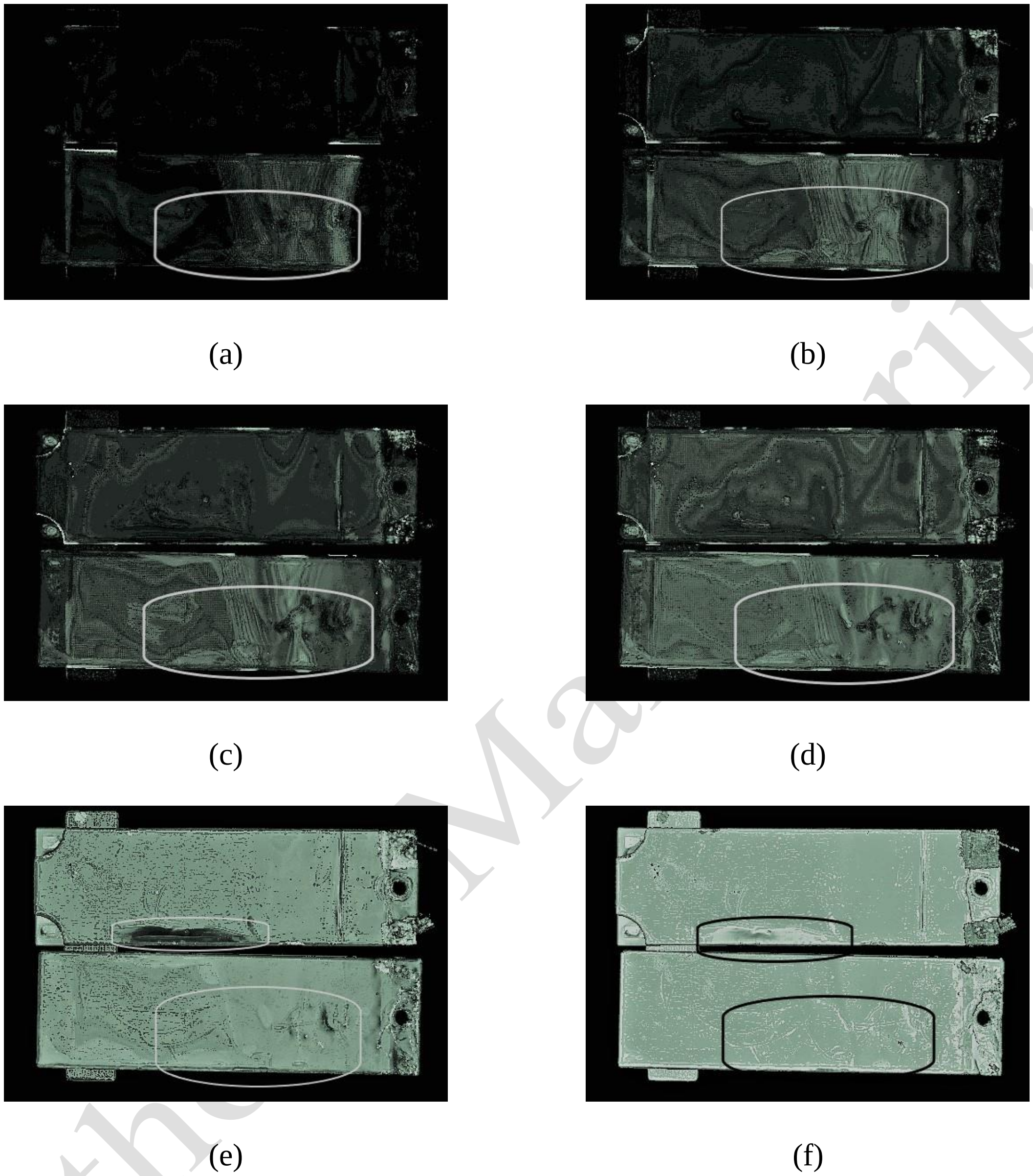


*Figure 7. Pristine (Top sample) and debonded (Bottom sample) samples scanned with ultrasonic waves through depth from the aluminum shim side (a) to (f).*

Figure 8 shows the frequency spectrum of RMS of the power generation for three replications. Firstly, the results obtained from the duplications are identical showing that the experiments are repeatable. As it can be seen from the frequency spectrum, there are two peaks for the output power at frequencies of 30 Hz and 49 Hz. The first peak frequency is related to the device fundamental bending natural frequency, while the second peak is result of anti-resonance frequency of the device. Anti-resonance frequency is the result of electromechanical coupling. At this frequency, the voltage and current are considerably different from resonance frequency even though the power is similar (DuToit et al., 2005).

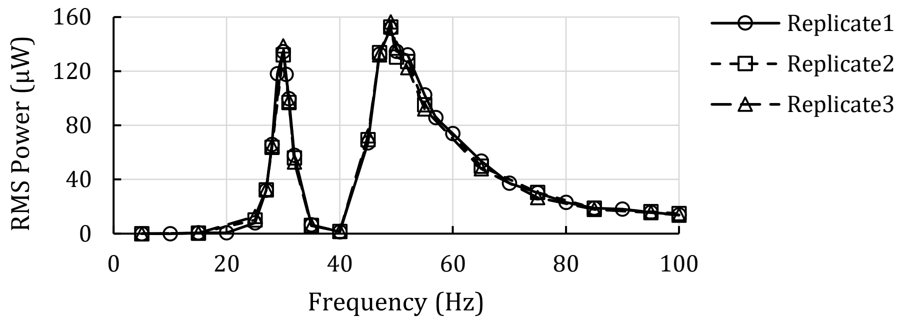


*Figure 8. Frequency spectrum of power for three replications on MFC sample*

The debonding reduces the active area in the device, which is an important factor in the power generation, and it increases the internal structural. Figure 9 shows the output power from the pristine and debonded samples as a function of frequency. Table 1 shows the variation of peak frequencies and output power between pristine and debonded samples. The debonding reduces the device stiffness and, hence, decreases the resonance and anti-resonance frequencies by 23 % and 18 %, respectively. Reductions in the peak frequencies are in the same order showing the stiffness reduction of the beam. Moreover, the presence of the debonding area causes a dramatic reduction in the output power at resonance and anti-resonance frequencies. There are two reasons for reduction of the power generation due to the debonding, reduction of the active area and increment in the damage damping. To measure the real debonding area, the debonded sample is exploited and the debonding region is marked, as shown in Figure 10. The debonding area is measured to be 15% of the active area. If a uniform generation of power assigned to the whole area, 15 % active area reduction will reduce output power by 15 %. Hence, the rest of the power reduction is due to increment of the damage damping. In addition, it can be noted from Figure 9 that, degradation of the output power is two times at the anti-resonance compared to at the power reduction at the resonance frequency, proving that the power at anti-resonance is much more sensitive to the debonding effect.

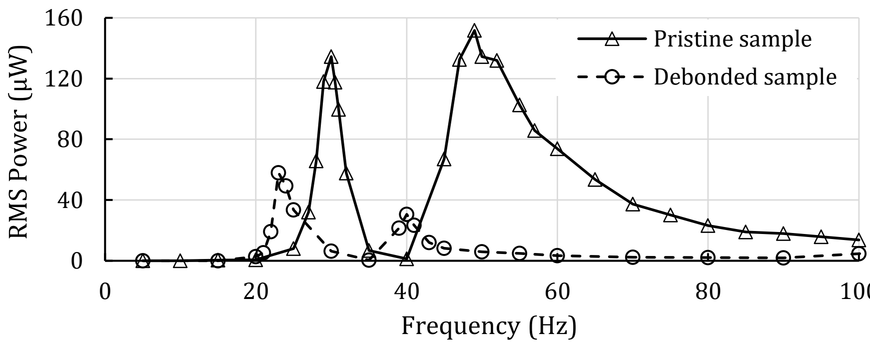


*Figure 9. Comparison between power for pristine and debonded samples over different frequencies*

*Table 1. Comparison between pristine and debonded samples*

| Parameter | Pristine | Debonded | Variation (%) |
|---|---|---|---|
| Resonance frequency (Hz) | 30 | 23 | -23.3 |
| Anti-resonance frequency (Hz) | 49 | 40 | -18.4 |
| RMS of power at resonance | 132.0 | 77.9 | -41.0 |
| RMS of power at anti-resonance | 152.7 | 30.5 | -80.0 |

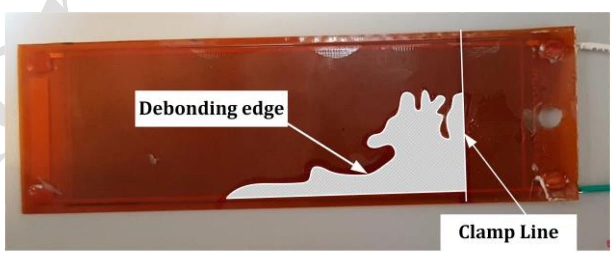


*Figure 10. Debonded area within adhesive and aluminum layer*

By applying the model presented by Eq. (3) and by updating the $\zeta_m$ through an error-minimization process, the analytical output power is correlated with respect to the experimental output power. This process is then repeated for the case that the debonding occurs by reduction of the active area. Figure 11 shows the comparison of the resonance power between the undamaged and bonded states based on the analytical and experimental results, and variation of the mechanical damping obtained after the model updating process. Figure 11 (a) shows that the power is successfully correlated at resonant by updating damping in the presented model. The presented model with correlation factor has better accuracy at resonant frequency compared to the other frequencies. However, as maximum available power is of interest in energy harvesting applications and this maximum power is obtained at resonant, the presented model can be used for maximum power correlation. Moreover, it can be seen from Figure 11 (a) that correlation for pristine sample is more accurate than for the debonded sample. This is due to the nonlinearity that is introduced into system due to debonding.  As shown in Figure 11 (b), correlated mechanical damping for the debonding sample shows that, the debonding caused to increase the $\zeta_m$ from 0.0483 to 0.0765. $\zeta_m$ comprises support loss, fluid-structural and internal friction damping mechanisms for defect-free state and damage damping for the case of deboned state. Fluid-structural damping are the same for both cases and will be evaluated using Eq. (5). Since during the tests boundary conditions remained unchanged, support loss are identical for both pristine and deboned states. However, since thickness of samples are slightly different for pristine and debonded samples, viscous damping coefficient was calculated for each condition. Damage damping was calculated by subtracting the calculated analytical fluid-structural, structural damping, experimentally obtained support loss damping from the correlated mechanical damping.

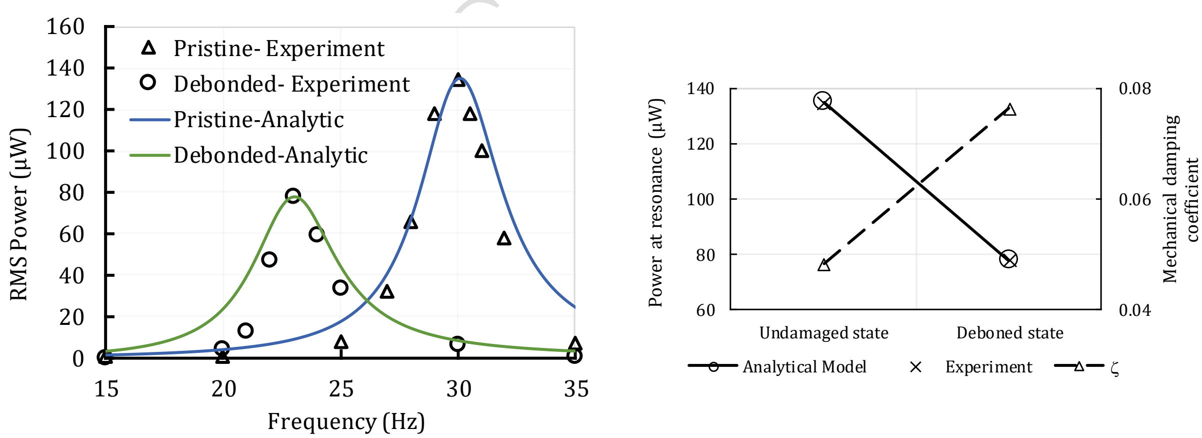


(a) (b)

*Figure 11. (a) Correlated data versus experimental data and (b) comparison between maximum power at resonance and damping increase due to debonding*

Table 2 summarizes the obtained results from this section. As it was shown previously, debonding area reduces 15% of the active area that is responsible for power generation. However, this 15% debonding area reduced the RMS resonant power density 20.53% from 60.83 to 48.34 μW/cm$^3$. Support loss, which is obtained by subtracting fluid-structure and structural damping from correlated damping coefficient, has a great contribution in the total damping proving that support loss damping is an important part of energy dissipation in the system and hence the next section is dedicated to this support loss. Damage damping in debonded sample is responsible for 27% of the total damping mechanisms showing that debonding can greatly affect damping coefficient.

*Table 2. Variation of output power, mechanical damping and structural damping due to improper bonding*

| Parameter | Undamaged sample | Debonded sample |
|---|---|---|
| Active area (cm$^2$) | 20.58 | 17.49 |
| RMS resonant power density (μW/cm$^3$) | 60.83 | 48.34 |
| $\zeta_m$ (Correlated value) | 4.83E-02 | 7.65E-02 |
| $\zeta_{Fluid\text{-}Structure}$ (Eq. (5)) | 7.90E-04 | 1.24E-03 |
| $\zeta_{Structural}$ (Eq. (5)) | 5.00E-07 | 5.00E-07 |
| $\zeta_{Support}$ ($=\zeta_m - \zeta_{Fluid\text{-}Structure} - \zeta_{Structural}$) | 4.75E-02 | 4.75E-02 |
| $\zeta_{Damage}$ ($=\zeta_m - \zeta_{Fluid\text{-}Structure} - \zeta_{Structural} - \zeta_{Support}$) | - | 2.78E-02 |

Nature of the damping variation due to delamination in the composite materials has been investigated by Khazaee et al. (Khazaee et al., 2018). The variation in damping depends on the vibrating mode, which causes penetration motion or slip motion between layers near the delamination (Khazaee et al., 2018). Fundamental mode shape of the unimorph harvester is shown in Figure 12. In this mode, if a debonding region is present, layers on top and bottom of the debonding area have a penetration motion in perpendicular direction causing an extra energy dissipation mechanism inside the harvesting material.

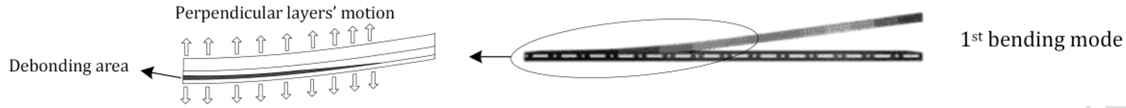


*Figure 12. Mechanical damping increases due to debonding in the first bending mode*

## 5. Support Loss Damping

Unimorph or bimorph is among the most applicable configuration of piezoelectric energy harvesters, where one end is clamped and the other end is free. To create the clamp, often a part of the energy harvester is clamped within a clamp box in which screws are tighten to provide non-moving area. Due to this clamp, an extra loss is introduced into the system, called support loss (Hosaka et al., 1995). In this section, output powers from a unimorph piezoelectric energy harvester under clamp-free boundary condition with different clamp box configuration are compared to each other in order to study the effect of the clamp characteristics on the output power.

Figure 12 (a) shows the sample for testing the support loss effect on the output power. The thickness of MFC piezoelectric, adhesive and substrate layers are 300, 245 and 120 µm, respectively. The clamp box consists of two 60×30 mm blocks with four screws placed symmetrically in the corners with 6 mm center-to-edge distance and one center hole for the shaker attachment. To observe the effect of the support loss, two types of materials were used for clamp box made by plastic and aluminum, as shown in Figure 13. The weight of clamp box set with screws for aluminum and plastic types are 59.09 g and 25.86 g, respectively. Moreover, the screws of clamp box were tighten with different torques and for each set of torque; the power was measured over a frequency range close to its natural frequency.

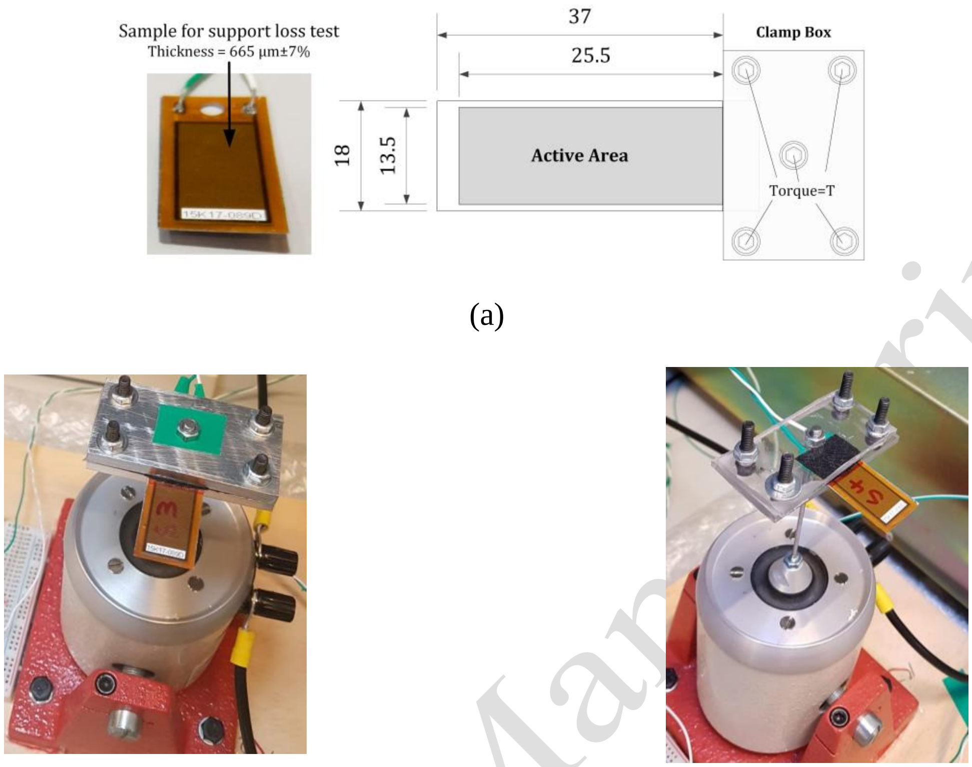


*Figure 13. (a) MFC harvester dimensions and unimorph configuration with clamp box screws, (b) Aluminum and (c) plastic clamp boxes clamping the MFC harvester*

Figure 14 shows the output power density in µW/g over a frequency range including the resonant frequency of piezoelectric energy harvester, where g= 9.81 m/s$^2$, from the MFC sample with the aluminum and plastic clamp boxes at different levels of tightening torques. The vertical axis shows the output power normalized to input base acceleration in terms of root mean square (RMS), when MFC sample were excited by a harmonic excitation with the maximum force of 17.8 N. For each case of excitation with the specific frequency, output voltage and current were measured with 31500-Ω resistance load and then power was calculated by product of voltage and current. Tightening torque, measured in N.m. unit, was the torque used for fastening the four screws of clamp box as well as the shaker attachment screw as shown in Figure 12 (a) and measured with the torque meter used for applying the torque. A sample of measured voltage, current and output power for plastic clamp box with tightening torque 0.5 N.m and excitation frequency of 220 Hz are shown in Figure 15. The immediate conclusion of Figure 14 is that, output power spectrums represent different values for different clamp box materials and tightening torques proving that clamping characteristics play an important role in energy harvesting from cantilevered piezoelectric beams. The resonant frequency, as displayed in Figure 16, for plastic clamp lies in the interval [212.1,220.4] Hz with an average of 215.8 Hz is higher than resonant frequency for aluminum clamp with an average of 199.5 Hz lying in the interval [198.4,202.1] H. Moreover, it can be seen that the tightening torque on the clamp box will change the output power of the energy harvester as well as slightly alters the resonant frequency of piezoelectric harvester. Output RMS power at resonance equals to 0.39 for T=0.5 N.m while this figure is 0.26 μW/g for T=0.8 N.m, when aluminum clamp box is used, showing a 33% reduction in output power due to tightening torque. This power reduction for plastic clamp box is 14% showing a lower dependency of power to tightening torque compared to aluminum clamp box. In addition, resonant frequency varies maximum 3.7% in the case of plastic clamp while this variation equals to maximum 1.7% for aluminum clamp.

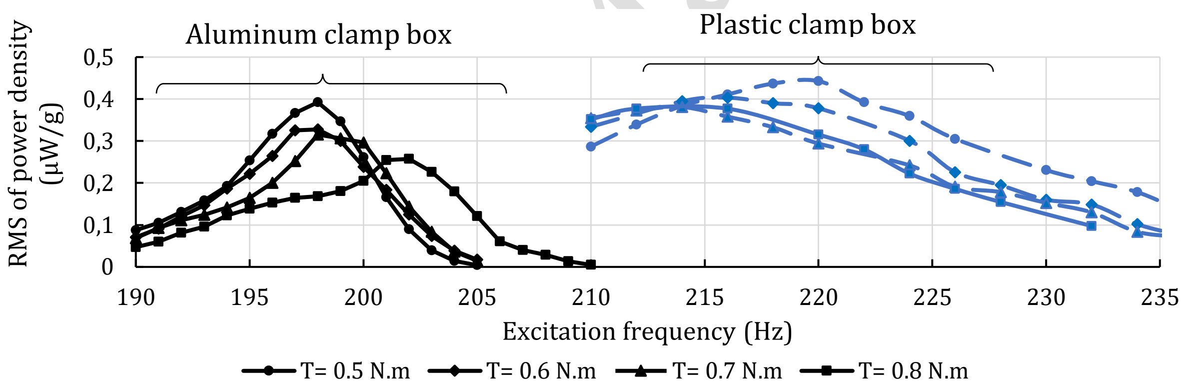


*Figure 14. Power frequency spectrum for sample 3 over changing torque T of aluminum clamp boxes*

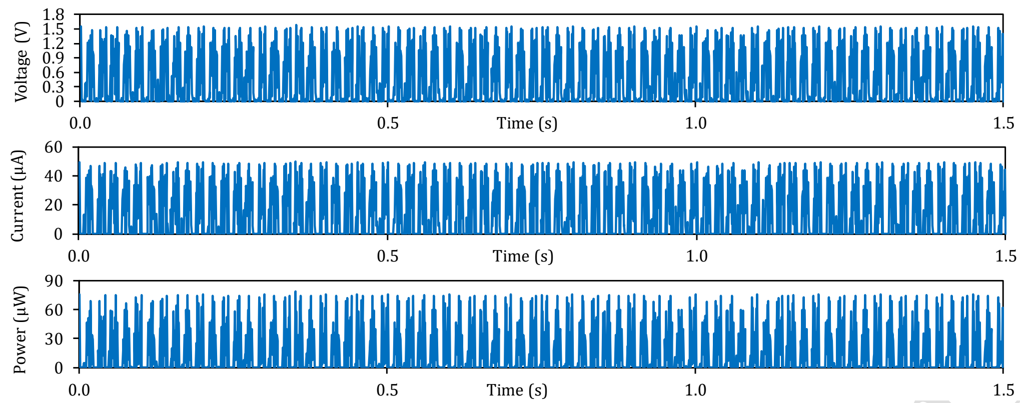


*Figure 15. Voltage, current and power from piezoelectric harvester with plastic clamp with T=0.5 N.m at 220 Hz excitation*

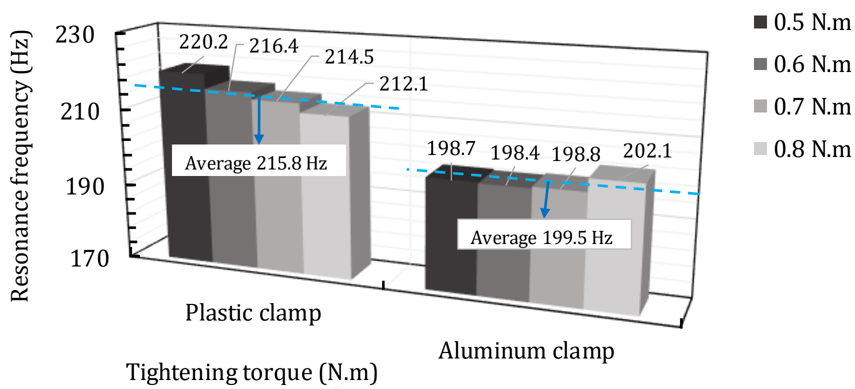


*Figure 16. Resonant frequency of piezoelectric harvester for different tightening torques on plastic and aluminum clamps*

Output current signals over a 1.5-second period from piezoelectric harvester with plastic clamp vibrating at its resonant frequency for different tightening torques are displayed in Figure 17. The RMS of output currents for tightening torques of 0.5, 0.6, 0.7 and 0.8 N.m are 23.8, 22.2, 21.9 and 21.7 µA showing that increasing tightening torque on cantilever clamp box reduces output current. Increasing tightening torque from 0.5 to 0.6 N.m reduced current by 6.7% while this drop is 1.4% for 0.6 to 0.7 N.m and 0.9% for 0.7 to 0.8 N.m tightening torque. Figure 18 shows the power at the resonance at different levels of tightening torque for the aluminum and plastic clamp boxes. Since the plastic clips have a degree of flexibility, to prove that the trend is reciprocal, the tests were performed from the lowest torque, T= 0.5 N.m, to the highest torque, T=0.8 N.m and vice versa. The results show that, the harvester with the aluminum clamp box produced lower power. On the other hand, by increasing the tightening torque of the screws of the clamp box, RMS of the maximum power decreases, for the both aluminum and plastic clamps. Figure 18 implies that, the plastic clips, which are more flexible than the aluminum, can provide higher output power and lower support loss compared to that one with the aluminum clamp.

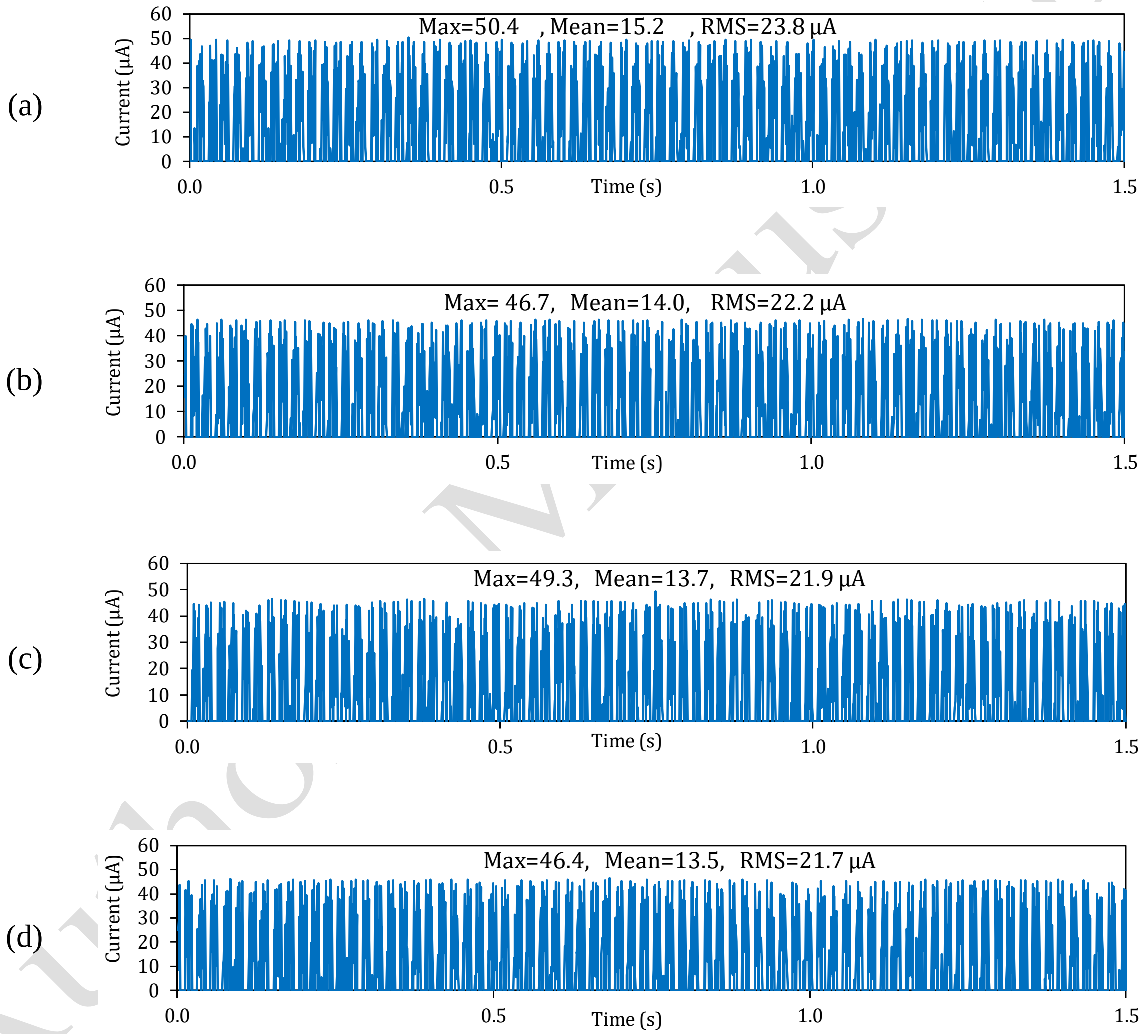


*Figure 17. Comparison between current measurements at resonant frequency excitation for plastic clamp at tightening torque (a) 0.5 N.m, (b) 0.6 N.m, (c) 0.7 N.m and 0.8 N.m*

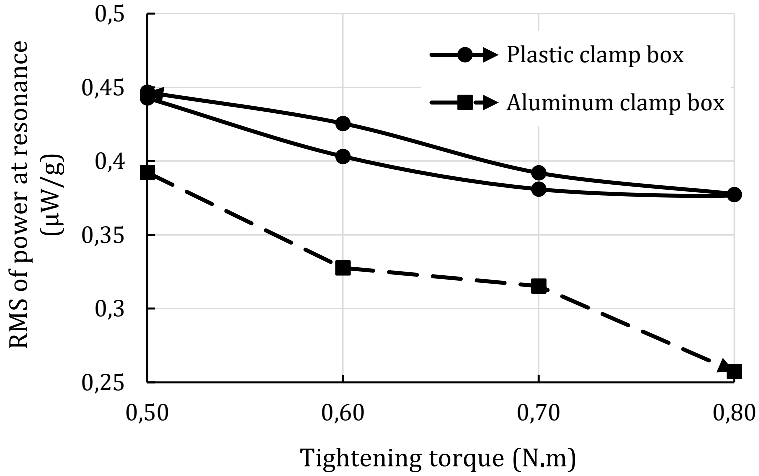


*Figure 18. Variation of power versus torque applied on clamp screws for different clamp box*

Similar to the previous section, using the developed model for the unimorph harvester, and with the minimization of the error between the maximum resonance powers, the mechanical damping ratios are identified for different clamp boxes at different tightening levels. These identified damping ratios are shown in Figure 19. Overall, aluminum clamp introduces higher energy dissipation, which in turn causes to reduce the damped natural frequency in Figure 14. Therefore, in comparison with the aluminum clamp box with higher support damping, the lower resonance frequency of the harvester with the plastic clamp box is due to lower support damping. However, with increasing the clamp pressure by higher tightening torque, the support loss increases for both clamp boxes, independent to clamp material.

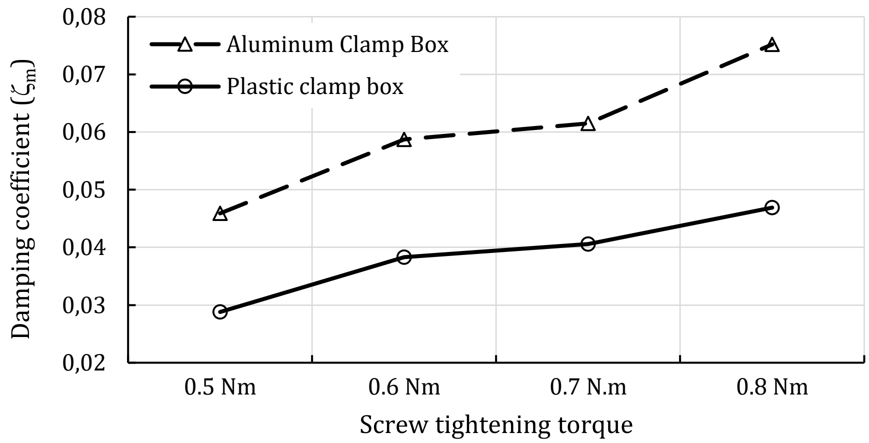


*Figure 19. Variations of identified damping variations versus clamp pressure for aluminum and plastic clamps*

## 6. Conclusions

This study presented an experimental investigation of effect of damage and support losses damping mechanisms on the output power of piezoelectric energy harvesters in unimorph geometry. The results show that, using a simple, but practical, single degree of freedom model, the power variation can be modelled with the mechanical damping variation. The debonding, as an internal source of damping inside the harvester, is investigated in this study. It is concluded that, the debonding increases the damping and reduces the output power dramatically. Moreover, the support loss, as an external damping source, has an effect on the output power in such a way that the clamp material as well as clamp pressure will change the output power.

## Declaration of Conflicting Interests

The author(s) declared no potential conflicts of interest with respect to the research, authorship, and/or publication of this article.

## References

Ahmed R, Mir F and Banerjee S (2017) A review on energy harvesting approaches for renewable energies from ambient vibrations and acoustic waves using piezoelectricity. *Smart Materials and Structures* 26(8). IOP Publishing: 085031. DOI: 10.1088/1361-665X/aa7bfb.

Bhattacharjee A and Nanda BK (2018) Damping study of composites using wavelet analysis. *JVC/Journal of Vibration and Control* 24(21): 5141–5151. DOI: 10.1177/1077546317745256.

Blom FR, Bouwstra S, Elwenspoek M, et al. (1992) Dependence of the quality factor of micromachined silicon beam resonators on pressure and geometry. *Journal of Vacuum Science & Technology B: Microelectronics and Nanometer Structures* 10(1): 19–26. DOI: 10.1116/1.586300.

Chandra R, Singh S p. and Gupta K (1999) Damping studies in fiber reinforced composites- a review. *Composite Structures* 46(1): 41–51.

Chen SY, Liu JZ and Guo FL (2017) Evaluation of support loss in micro-beam resonators: A revisit. *Journal of Sound and Vibration* 411. Elsevier Ltd: 148–164. DOI: 10.1016/j.jsv.2017.08.048.

DuToit NE and Wardle BL (2007) Experimental Verification of Models for Microfabricated Piezoelectric Vibration Energy Harvesters. *AIAA Journal* 45(5): 1126–1137. DOI: 10.2514/1.25047.

DuToit NE, Wardle BL and Kim SG (2005) Design considerations for MEMS-scale piezoelectric mechanical vibration energy harvesters. *Integrated Ferroelectrics* 71: 121–160. DOI: 10.1080/10584580590964574.

Erturk a, Bilgen O, Fontenille M, et al. (2008) Piezoelectric energy harvesting from macro-fiber composites with an application to morphing wing aircrafts. *Proceedings of the 19th International Conference of Adaptive Structures and Technologies*.

Erturk A and Inman DJ (2008) Issues in mathematical modeling of piezoelectric energy harvesters. *Smart Materials and Structures* 17(6). DOI: 10.1088/0964-1726/17/6/065016.

Goyder HGD (2018) Damping Due to Joints in Built-Up Structures. In: Brake MRW (ed.) *The Mechanics of Jointed Structures: Recent Research and Open Challenges for Developing Predictive Models for Structural Dynamics*. Cham: Springer International Publishing, pp. 135–147. DOI: 10.1007/978-3-319-56818-8_11.

Hao Z, Erbil A and Ayazi F (2003) An analytical model for support loss in micromachined beam resonators with in-plane flexural vibrations. *Sensors and Actuators, A: Physical* 109(1–2): 156–164. DOI: 10.1016/j.sna.2003.09.037.

Hosaka H, Itao K and Kuroda S (1995) Damping characteristics of beam-shaped micro-oscillators. *'Sensors and Actuators, A: Physical'*. DOI: 10.1016/0924-4247(95)01003-J.

Https://www.piezotech.eu (n.d.) PiezeTech Arkema Group.

Ibrahim RA and Pettit CL (2005) Uncertainties and dynamic problems of bolted joints and other fasteners. *Journal of Sound and Vibration* 279(3–5): 857–936. DOI: 10.1016/j.jsv.2003.11.064.

Khaligh A, Zeng P and Zheng C (2010) Kinetic Energy Harvesting Using Piezoelectric and Electromagnetic Technologies; State of the Art. *Industrial Electronics, IEEE Transactions on* 57(3): 850–860. DOI: 10.1109/TIE.2009.2024652.

Khazaee M, Nobari AS and Aliabadi MHF (2018) *Experimental Investigation of Delamination Effects on Modal Damping of a CFRP Laminate, Using a Statistical Rationalization Approach*. *Computational and Experimental Methods in Structures*. DOI: 10.1142/9781786344977_0003.

Khazaee M, Rezaniakolaei A and Rosendahl L (2019) An experimental study on macro Piezoceramic fiber composites for energy harvesting. *Materials Science Forum* 951: 3–8. DOI: https://doi.org/10.4028/www.scientific.net/MSF.951.3.

Li H, Tian C and Deng ZD (2014) Energy harvesting from low frequency applications using piezoelectric materials. *Applied Physics Reviews* 1(4): 0–20. DOI: 10.1063/1.4900845.

Mortazavinatanzi S, Rezaniakolaei A and Rosendahl L (2018) Printing and folding: A solution for high-throughput processing of organic thin-film thermoelectric devices. *Sensors (Switzerland)* 18(4): 989. DOI: 10.3390/s18040989.

Pazand K and Nobari AS (2017) Investigation of damage effect on the effective dynamic mechanical properties of an adhesive in linear and nonlinear response regimes. *Journal of Vibration and Control* 23(14). DOI: 10.1177/1077546315612904.

Qing S, Rezania A, Rosendahl LA, et al. (2018) Characteristics and parametric analysis of a novel flexible ink-based thermoelectric generator for human body sensor. *Energy Conversion and*

*Management* 156: 655–665. DOI: 10.1016/j.enconman.2017.11.065.

Reddy AR, Umapathy M, Ezhilarasi D, et al. (2016) Improved energy harvesting from vibration by introducing cavity in a cantilever beam. *JVC/Journal of Vibration and Control* 22(13): 3057–3066. DOI: 10.1177/1077546314558498.

Roundy S, Wright PK and Rabaey J (2003) A study of low level vibrations as a power source for wireless sensor nodes. *Computer Communications* 26(11): 1131–1144. DOI: 10.1016/S0140-3664(02)00248-7.

Saravanos D a. and Hopkins D a. (1996) Effect of delamination on the damped dynamic characteristics of composite laminates. analysis and experiments. *Journal of Sound and Vibration* 192(2): 977–993. DOI: 10.1006/jsvi.1996.0229.

Shan X, Song R, Liu B, et al. (2015) Novel energy harvesting: A macro fiber composite piezoelectric energy harvester in the water vortex. *Ceramics International* 41(S1). Elsevier: S763–S767. DOI: 10.1016/j.ceramint.2015.03.219.

Sodano HA, Lloyd J and Inman DJ (2006) An experimental comparison between several active composite actuators for power generation. *Smart Materials and Structures* 15(5): 1211–1216. DOI: 10.1088/0964-1726/15/5/007.